FRI MODELLING OF FOURIER DESCRIPTORS

Abijith Jagannath Kamath

Department of Electrical and
Electronics Engineering
National Institute of Technology Karnataka
Surathkal - 575025, India
kamath.abijith.j@ieee.org

Sunil Rudresh, Chandra Sekhar Seelamantula

Department of Electrical Engineering
Indian Institute of Science
Bangalore - 560012, India
sunilr@iisc.ac.in, chandra.sekhar@ieee.org

ABSTRACT

Fourier descriptors are used to parametrically represent closed contours. In practice, a finite set of Fourier descriptors can model a large class of smooth contours. In this paper, we propose a method for estimating the Fourier descriptors of a given contour from its partial samples. We take a sampling-theoretic approach to model the x and y coordinate functions of the shape and express them as a sum of weighted complex exponentials, which belong to the class of finite-rate-of-innovation (FRI) signals. The weights represent the Fourier descriptors of the shape. We use the FRI framework to estimate the shape parameters reliably from noisy and partial measurements. We model non-uniformities in sampling using the sampling jitter model and employ a prefiltering process to reduce the effect of measurement noise and jitter. The average sampling interval is estimated by a block annihilating filter, which is then followed by the estimation of Fourier descriptors using least-squares fitting. We demonstrate the robustness of the proposed algorithm to noise and sampling jitter. Monte Carlo performance analysis shows that the variances of the estimators are close to the Cramér-Rao lower bounds. We present results for outlining shapes in synthetic as well as real images.

***Index Terms*—** Fourier descriptors, finite-rate-of-innovation signals, block annihilation, parametric curves.

1. INTRODUCTION

Shape reconstruction or shape parameterization is crucial in numerous image processing, computer vision, and pattern recognition applications. Shape parameters are used as features for object matching and classification [1], and they also provide a succinct representation of the data. One such parameterization of shapes with closed contours is given by Fourier descriptors [2]. Fourier descriptors (FDs) of a closed curve $C : \{x(t), y(t)\}$, which may represent the boundary of an object in an image are the coefficients in the Fourier series expansion of an analytic function constructed as $s_C(t) = x(t) + \mathrm{j}y(t)$:

$$s_C(t) = \sum_{k\in\mathbb{Z}} c_k \, e^{\mathrm{j}kt}, \quad c_k \in \mathbb{C}. \tag{1}$$

A truncated set of coefficients $\{c_k\}_{k=-K}^{K}$ approximates $s_C(t)$ to an order K and this finite set of coefficients represents a broad class of smooth shapes. Given FDs of a closed contour, the FDs of translated, rotated, sheared, or scaled versions of the contour can be readily obtained as several interesting and simple relations exist between the geometry of shapes and algebraic properties of the FDs [3]. Owing to such attractive features, FDs have found several applications such as in shape matching and discrimination in the field of pattern recognition [4–6] and image processing for medicine and biology [7]. An Illustration of outlining of tumours using the proposed method is shown in Fig. 1. Many parametric models including FDs rely on inverse transforms for reconstruction, often requiring a complete set of measurements on the closed contour, which might not be available due to poor pre-processing, low resolution, occlusion etc. Clustering-based techniques such as Hough transform [8] are robust to outliers, but they are computationally intensive. The complexity of such algorithms increases significantly as the order K increases. In practice, for real images, shapes are represented by points drawn from the contour of an object. Generally, an edge detection algorithm is applied on the grey-scale image and a set of uniformly-spaced pixels on the edge location are selected as points on the contour. Since images are discretized spatially, the selected pixels may not correspond to uniform samples of the contour resulting in what is known as *sampling jitter*.

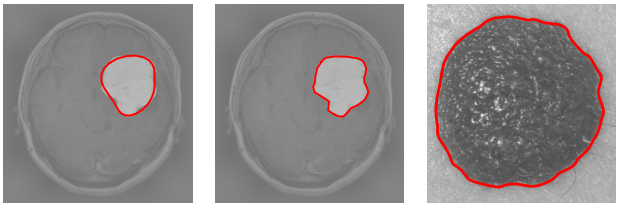

(a) $K = 3, N = 31$ (b) $K = 13, N = 31$ (c) $K = 24, N = 460$

Fig. 1: [Colour online] Outlining (curves in red) of tumours in T1 contrast enhanced brain MRI [9, 10] and images of melanoma [11] using the proposed method. Approximation near the regions having high curvature gets better with increasing model order.

This Paper: We propose a novel finite-rate-of-innovation (FRI) signal [12] model for closed contours and regard FDs as the degrees of freedom of the signal in (1). A finite set of FDs can characterize a large class of smooth closed contours, which implies that $s_C(t)$ has finite number of degrees of freedom and hence can be modelled as an FRI signal as shown in Section 2. As a particular case, for $K = 1$, the curve C represents an ellipse. We have shown in [13] that the FRI modelling of ellipse is a robust approach for its representation and reconstruction as compared with several state-of-the-art ellipse fitting techniques. Complex shapes of higher orders can be approximated by taking a larger set of coefficients by increasing the value of K, thus generalizing the ellipse model. The fact that, in the absence

The authors would like to thank the Science and Engineering Research Board (SERB), Government of India for funding this work.

of noise, an FRI signal with K degrees of freedom is completely represented by a minimum of $2K$ measurements [12] is significant as it enables one to represent an FRI contour with partially available sample points. In Section 3, we employ high-resolution spectral estimation techniques [14], in particular, the annihilating filter [15] to estimate the parameters. Also, in the presence of noise, we perform prefiltering of the noisy samples before estimating the FDs. In our earlier work, we showed that prefiltering the samples with a lowpass kernel reduces the variance of the random amplitude modulation on the FDs caused by the jitter [13]. In Section 4, we analyze the noise robustness of the proposed method and show that the variances in the estimated parameters meet the corresponding Cramér-Rao lower bounds (CRLBs). The squared bias in the estimation of parameters is as low as -60 dB at SNR of 0 dB. We also present the performance of the proposed method on synthetic curves as well as real images.

Other FRI Models for Curve Fitting: Recently, Pan et al. [16] proposed a method to sample and reconstruct curves by extending the FRI principle to curves in 2D. The authors showed that the finite coefficients of a parameterized mask function annihilate the Fourier transform of the derivative of the edge image. The curve representation is implicit and relies on the level-set of a mask function. Ongie and Jacob extended the formulation in [16] to accommodate natural images along with robust reconstruction techniques, and successfully demonstrated super-resolution magnetic resonance imaging (MRI) as an application [17–19]. If a parametric curve is occluded, the mask function based method would reconstruct only a part of the curve that is not occluded along with the boundary of the occluding object. Hence, reconstruction of closed contours from partial measurements is not possible. Therefore, we choose to explicitly model the contours as FRI objects with sampling interval and FDs as parameters. Thus, the measurement model and the signal model in the proposed technique are different from that of [16]. On the other hand, the proposed method can only handle one curve at a time unlike the approaches presented in [16–19].

2. FOURIER DESCRIPTORS ARE FRI CURVES

Consider the explicit parametric representation of a curve, which is the closed boundary of a shape represented as $C : \{x(t), y(t)\}$ using Fourier descriptors as in (1) with a finite model order K. Uniform samples of x and y coordinates of C, sampled at an interval T result in a sum of weighted complex exponentials (SWCE):

$$x(t)|_{t=nT} = \sum_{k=-K}^{K} \alpha_k \, e^{\mathrm{j}knT} \text{ and } \quad y(t)|_{t=nT} = \sum_{k=-K}^{K} \beta_k \, e^{\mathrm{j}knT}, \quad (2)$$

respectively. We enforce the constraints $\alpha_k = \alpha_{-k}^*$ and $\beta_k = -\beta_{-k}^*$ to ensure real x and purely imaginary y coordinate functions so that our model agrees with the standard FD model in (1). Further, a combination of the weights $c_k = \alpha_k + \mathrm{j}\beta_k, \ \forall \ k \in \mathcal{K} = \{-K, -K+1, \cdots, K-1, K\}$ gives the Fourier descriptors of the curve C. The parameter set $\mathbf{\Theta} = [T \ c_{-K} \ \cdots \ c_0 \ \cdots \ c_K]$ completely describes the curve C. Suppose we obtain N noisy, ordered measurements $\{\tilde{x}(nT), \tilde{y}(nT)\}_{n=1}^{N}$ with $NT \leq 2\pi$ such that $\tilde{x}(nT) = x(nT) + w_x(n)$ and $\tilde{y}(nT) = y(nT) + w_y(n)$, where the sequences $\{w_x(n)\}_{n=1}^{N}$ and $\{w_y(n)\}_{n=1}^{N}$ are modelled as independent and identically distributed (i.i.d.) Gaussian noise samples with zero mean and variance σ^2. We seek to estimate the parameter set $\mathbf{\Theta}$ from the full or partial set of measurements $\{\tilde{x}(nT), \tilde{y}(nT)\}$.

3. PARAMETER ESTIMATION OF FRI CURVES

Sampling and reconstruction of FRI signals, in particular, a stream of Dirac impulses proposed by Vetterli et al. [12] has been extended to a stream of periodic and aperiodic pulses by Tur et al. [20] with ultrasound imaging as an application. Subsequently, FRI signal sampling has found applications in super-resolution imaging [16, 17, 21–23] and curve fitting [13]. In these applications, the measurements are transformed into a domain such that the signal is completely characterized by a SWCE, where the exponents and weights form the parameter set that has to be estimated. The signal models in (2) are FRI signals with a total of $2(K+1)$ number of parameters and they are already in the form of a SWCE, where T is the unknown *sampling interval*. Robust estimation of T by employing block annihilation allows for estimation of the weights $\{\alpha_k, \beta_k\}$ using a least-squares minimization approach.

3.1. Estimation of Sampling Interval

The annihilating filter or Prony's algorithm [15] is a HRSE method that is used to estimate the parameters of a SWCE signal instead of nonlinear least-squares minimization. The authors in [13] chose either $x(nT)$ or $y(nT)$, whichever has a higher signal-to-noise ratio (SNR), as input to the annihilating filter. In order to make use of all the available measurements, we employ the block annihilation scheme originally proposed in [24]. It ensures unbiased estimation of T using both the x and y measurements. We found that this also gives a more robust estimate as compared with the method used in [13]. We obtain two sequences with the common complex exponential support in $x(nT)$ and $y(nT)$. We are interested in a causal, finite-impulse-response (FIR) filter $h(n)$ of the order $2K+1$, with a $\mathcal{Z}$-transform $H(z) = \prod_{k=-K}^{K} (1 - e^{\mathrm{j}kT} z^{-T})$. The filter outputs $(x * h)(n)$ and $(y * h)(n)$ vanish for $(2K+1) \leq n \leq N-(2K+1)$, i.e., the filter $h(n)$ annihilates the sequences $x(nT)$ and $y(nT)$. The zeros of the filter are $\{e^{\mathrm{j}kT}\}_{k=-K}^{K}$, from which $\{kT\}_{k=-K}^{K}$ have to be computed, whose smallest non-zero positive value is taken as the estimated sampling interval. To determine the filter, the convolution is written in the matrix form as $\mathbf{Xh} = \mathbf{0}$ and $\mathbf{Yh} = \mathbf{0}$, where $\mathbf{X}$ and $\mathbf{Y}$ are the convolution matrices constructed from $\{x(nT)\}$ and $\{y(nT)\}$, respectively. We construct a block matrix $\mathbf{U}$ and find a common $\mathbf{h} = [h_0 \ h_1 \cdots h_{2K}]^{\mathrm{T}}$ that lies in the null space of both $\mathbf{X}$ and $\mathbf{Y}$:

$$\mathbf{Uh} = \begin{bmatrix} \mathbf{X} \\ \mathbf{Y} \end{bmatrix} \mathbf{h} = \mathbf{0}. \quad (3)$$

In the presence of noise, $\mathbf{U}$ may end up being full rank and perfect annihilation might not be possible. In this case, we first denoise the samples and find an approximate solution to (3) as:

$$\arg\min_{\mathbf{h}} ||\mathbf{Uh}||_2^2 \text{ subject to } ||\mathbf{h}||_2^2 = 1.$$

We solve for $\mathbf{h}$ using a Yule-Walker solver or by taking the right singular vector corresponding to the smallest singular value of $\mathbf{U}$.

3.2. Denoising Using Prefiltering

For robust estimation of the sampling interval, we use a lowpass filter to denoise the samples and consequently identify the best annihilating filter in the approximate null space of $\mathbf{U}$. A lowpass filter also reduces the effect of sampling jitter in the case of nonuniform sampling [13]. For a curve of order K, the curve-specific information is available only in the interval $[-KT, KT]$ and we wish to suppress

the samples outside this interval. Consider an M-tap lowpass filter $f(nT)$ with a cut-off frequency close to KT. The signal $\tilde{x}(nT)$ is filtered using $f(nT)$ resulting in:

$$(\tilde{x} * f)(n) \approx \alpha_0 F(0) + \sum_{k=1}^{K} \left[F(kT)\alpha_k \, e^{\mathrm{j}knT} + F(-kT)\alpha_k^* \, e^{-\mathrm{j}knT} \right],$$

where $F(\omega) = \sum_{n=0}^{M-1} f(n) e^{-\mathrm{j}\omega n}$ is the frequency response of the lowpass filter. We observe that the lowpass filtering scales the k^{th} Fourier descriptor by a factor of $F(kT)$ while suppressing the noise. To reliably recover the weights, we require the scaling factors to satisfy $F(kT) \approx 1$. Also, larger the filter length M, the better is the denoising for a fixed cutoff frequency as the frequency response of the lowpass filter rolls off quickly. However, this reduces the effective number of available samples in the SWCE form for the estimation of the sampling interval. Hence, there is a trade-off between the filter length and the cutoff frequency to ensure optimal denoising. In the simulation results presented in this paper, we have used the Tukey window with parameter 0.99 and length $M = \left\lfloor \frac{2N}{3} \right\rfloor$.

3.3. Estimation of Fourier Descriptors

The coefficients $\mathbf{a} = [\alpha_{-K} \;\; \alpha_{-K+1} \;\; \cdots \;\; \alpha_{K-1} \;\; \alpha_K]^{\mathrm{T}}$ and $\mathbf{b} = [\beta_{-K} \;\; \beta_{-K+1} \;\; \cdots \;\; \beta_{K-1} \;\; \beta_K]^{\mathrm{T}}$, which form the FDs are obtained as the least-squares solution to $\mathbf{Ea} = \tilde{\mathbf{x}}$ and $\mathbf{Eb} = \tilde{\mathbf{y}}$, where $\tilde{\mathbf{x}}$ and $\tilde{\mathbf{y}}$ are the vectors formed using the denoised sequences $\{\tilde{x}(n)\}$ and $\{\tilde{y}(n)\}$, respectively, and $\mathbf{E}$ is a Vandermonde matrix constructed as follows:

$$\mathbf{E} = \begin{pmatrix} e^{-\mathrm{j}KT} & \cdots & e^{-\mathrm{j}T} & 1 & e^{jT} & \cdots & e^{\mathrm{j}KT} \\ e^{-\mathrm{j}2KT} & \cdots & e^{-\mathrm{j}2T} & 1 & e^{\mathrm{j}2T} & \cdots & e^{\mathrm{j}2KT} \\ \vdots & \ddots & \vdots & \vdots & \vdots & \ddots & \vdots \\ e^{-\mathrm{j}NKT} & \cdots & e^{-\mathrm{j}NT} & 1 & e^{\mathrm{j}NT} & \cdots & e^{\mathrm{j}NKT} \end{pmatrix}.$$

We refer to the proposed technique as the FRI-FD method.

4. EXPERIMENTAL RESULTS

4.1. Noise Robustness

We present the performance analysis of the proposed method in the presence of noise. Consider the signal model:

$$\tilde{\mathbf{x}} = \mathbf{Ea} + \mathbf{w}, \quad \tilde{\mathbf{y}} = \mathbf{Eb} + \mathbf{w},$$

where the matrix $\mathbf{E}$ depends on the parameter T and $\mathbf{w} \sim \mathcal{N}(0, \sigma^2 \mathbf{I})$. We compute the mean-squared error (MSE) in the estimation of $\mathbf{a}$, $\mathbf{b}$, and T. Consider samples from a curve of model order $K = 1$ with parameters $T = 0.01$, $\alpha_0 = 2$, $\alpha_1 = \alpha_{-1} = 8$, $\beta_0 = 3$, and $\beta_1 = -\beta_{-1} = 7$. A total of $N = 629$ noisy samples are generated and denoised using a lowpass filter, a Tukey window with parameter 0.99 and cutoff frequency of 0.015 radians. For each SNR, the MSE values are averaged over 5000 independent noise realizations. The SNR is computed as $\frac{1}{\sigma^2} \sum_{n=1}^{N} \left(|x(nT)|^2 + |y(nT)|^2 \right)$.

To compute the Cramér-Rao lower bound on the variance of the parameter estimators, we construct the Fisher information matrix of the parameters $\mathbf{\Theta} = [T \;\; \theta_{\mathbf{p}}]^{\mathrm{T}}$ as

$$I(\mathbf{\Theta}) = -\mathbb{E}\Big[\frac{\partial^2 \ell(\mathbf{z};\Theta)}{\partial \mathbf{\Theta}^2}\Big] = -\mathbb{E}\begin{bmatrix} \frac{\partial^2 \ell(\mathbf{z};\mathbf{\Theta})}{\partial T^2} & \frac{\partial^2 \ell(\mathbf{z};\mathbf{\Theta})}{\partial \theta_{\mathbf{p}}{}^{\mathrm{T}} \partial T} \\ \frac{\partial^2 \ell(\mathbf{z};\mathbf{\Theta})}{\partial T \partial \theta_{\mathbf{p}}{}^{\mathrm{T}}} & \frac{\partial^2 \ell(\mathbf{z};\mathbf{\Theta})}{\partial \theta_{\mathbf{p}} \partial \theta_{\mathbf{p}}{}^{\mathrm{T}}} \end{bmatrix},$$

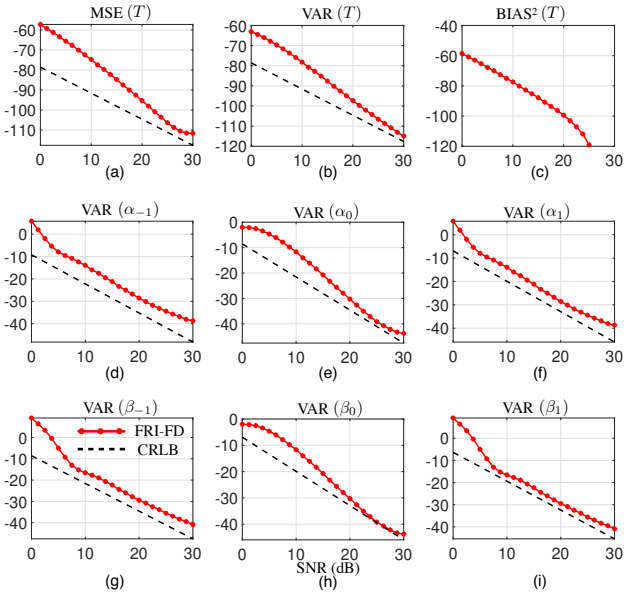

Fig. 2: Bias, variance, and MSE of the estimated parameters of a closed contour of model order $K = 1$. Both axes are in dB scale. The results are obtained by averaging estimates from 5000 independent Monte Carlo realizations. Bias values for the other parameters were found to be less than -70 dB.

where $\ell(\mathbf{z};\mathbf{\Theta})$ is the likelihood function of the measurements $\mathbf{z} = [\mathbf{x} \; \mathbf{y}]^{\mathrm{T}}$ corrupted by zero-mean, additive white Gaussian noise with variance σ^2 and $\theta_{\mathbf{p}} = [\alpha_{-K} \cdots \alpha_0 \cdots \alpha_K \; \beta_{-K} \cdots \beta_0 \cdots \beta_K \;]^{\mathrm{T}}$. The entries of the Fisher matrix are computed as:

$$\mathbb{E}\left[\frac{\partial^2 \ell(\mathbf{z};\mathbf{\Theta})}{\partial \theta_{\mathbf{p}} \partial \theta_{\mathbf{p}}{}^{\mathrm{T}}}\right] = \frac{-1}{\sigma^2} \bar{\mathbf{E}}^H \bar{\mathbf{E}}, \text{ where } \bar{\mathbf{E}} = \begin{bmatrix} \mathbf{E} & \mathbf{0} \\ \mathbf{0} & \mathbf{E} \end{bmatrix},$$

$$\mathbb{E}\left[\frac{\partial^2 \ell(\mathbf{z};\mathbf{\Theta})}{\partial \alpha_k \partial T}\right] = \frac{-1}{\sigma^2} \sum_{n=1}^{N} \left[e^{\mathrm{j}knT} \left(\sum_{k=-K}^{K} \alpha_k \mathrm{j}kn e^{\mathrm{j}knT} \right) \right],$$

$$\mathbb{E}\left[\frac{\partial^2 \ell(\mathbf{z};\mathbf{\Theta})}{\partial \beta_k \partial T}\right] = \frac{-1}{\sigma^2} \sum_{n=1}^{N} \left[e^{\mathrm{j}knT} \left(\sum_{k=-K}^{K} \beta_k \mathrm{j}kn e^{\mathrm{j}knT} \right) \right], \text{ and}$$

$$\mathbb{E}\left[\frac{\partial^2 \ell(\mathbf{z};\mathbf{\Theta})}{\partial T^2}\right] = \frac{-1}{\sigma^2} \sum_{n=1}^{N} \left[\left(\sum_{k=-K}^{K} \alpha_k \mathrm{j}kn e^{\mathrm{j}knT} \right)^2 + \left(\sum_{k=-K}^{K} \beta_k \mathrm{j}kn e^{\mathrm{j}knT} \right)^2 \right].$$

The CRLBs of the variances of unbiased estimators of parameters are the corresponding diagonal entries of the inverse of $I(\mathbf{\Theta})$. Figures 2(a)-(c) show bias, variance, and MSE in the estimation of T. It is observed that the squared bias of the estimator is as low as -60 dB at SNR of 0 dB and the variance almost meets the CRLB around SNR of 20 dB. The variances in the estimation of FDs are shown in Figs. 2(d)-(i). It has been observed that the bias curves for the FDs follow the same trend as that of T. Accuracy of estimates of the weights is dependent on the estimation of the sampling interval and hence, the variances of estimators of all the FDs meet the CRLBs at SNRs where the sampling interval is accurately estimated.

4.2. Synthetic Curves and Real Images

We consider reconstruction of shape boundaries from noisy measurements. Figures 3(a)-(f) show the reconstruction of closed contours of order $K = 2$ with the full and partial (60%) set of measurements used for parameter estimation. Similarly, Figs. 3(g)-(l) show the reconstructions for a contour of order $K = 3$. In both the

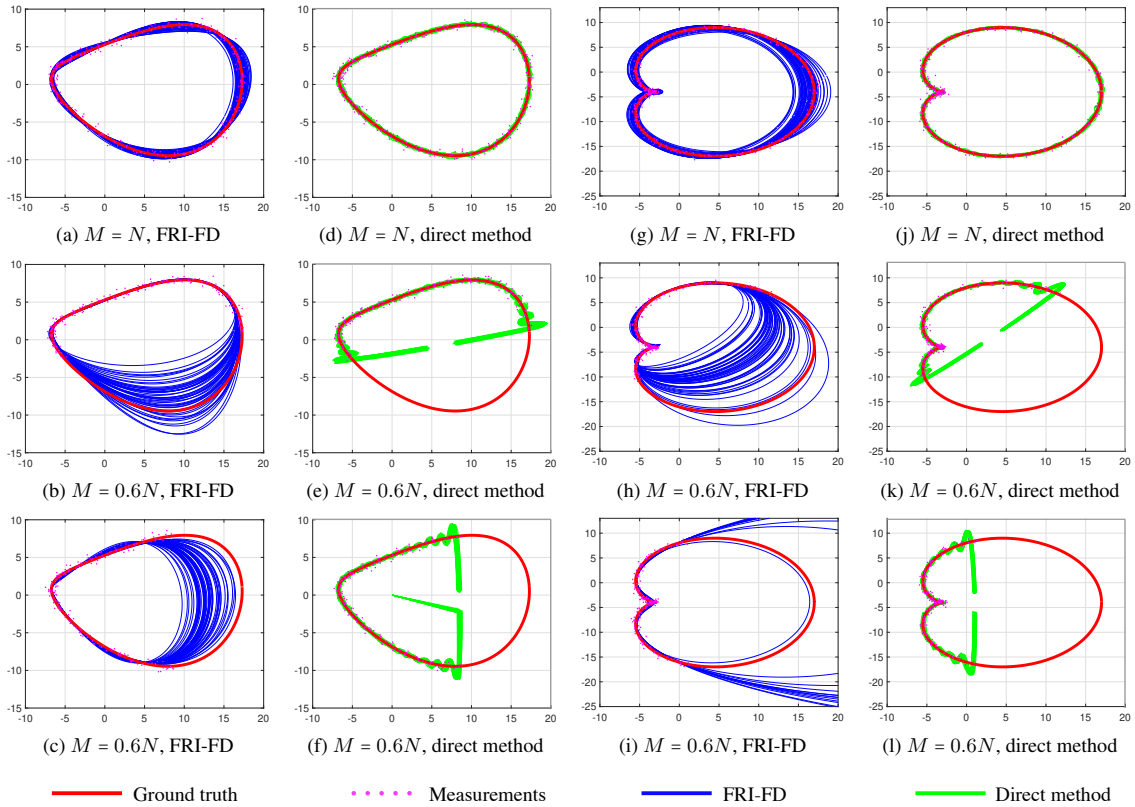

Fig. 3: [Colour online] The reconstruction of contours of order (a)-(f) $K = 2$ and (g)-(l) $K = 3$ at SNR = 20 dB. The first row shows the reconstructions obtained using the full set of measurements, whereas the second and third rows show reconstruction using partial set of measurements. For both FRI-FD and direct methods, the reconstructed contours from 50 noise realizations are overlaid.

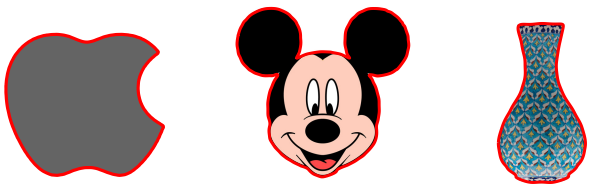

(a) $K = 100, N = 340$ (b) $K = 68, N = 505$ (c) $K = 25, N = 345$

Fig. 4: [Colour online] Illustration of FRI-FD to outline (in red) closed contours of different shapes. More complex contours can be approximated by using a larger model order.

cases, $N = 126$ noisy samples at SNR of 20 dB are generated with $T = 0.05$. The second and third rows correspond to reconstruction using partial samples that are taken from two different regions of the contours. It is observed that if the partial samples are not taken from regions with a high curvature, the proposed method fails to reliably reconstruct the contour as the model order must be high for such regions and correspondingly, more samples must be acquired (see Fig. 3(i)). The second and fourth columns show the results for reconstruction performed using the direct method, i.e., by Fourier inversion of FDs that are obtained using the full or partial set of measurements. The direct method is able to give a reliable reconstruction only if the FDs are obtained using the full set of measurements. Modifications to the direct method have been made to accommodate for missing samples, but the performance is reliable only if the percentage of missing samples is less than 20% and requires a priori estimation of N [25]. Figure 1 in Section 1 shows reconstruction results on real images (brain MRI and melanoma) obtained from data sets in [9–11], which contain ordered points that are handpicked on the boundaries of tumours. In the case of unavailability of the boundary and ordering information, we employ Canny's algorithm [26] to detect the edge contours and approximate solutions to the Travelling Salesman Problem for ordering the samples. Reconstruction results on some of the real images using a full set of measurements are shown in Fig. 4.

5. CONCLUSIONS

We proposed the FRI signal model for characterizing smooth closed contours with Fourier descriptors as parameters. This generalizes the ellipse fitting model in [13] to a larger class of smooth contours. Since the contours are modelled as FRI signals, it facilitates computation of Fourier descriptors of a shape from partial or incomplete measurements of the coordinate functions. Application of the block annihilating filter, which uses both the x and y coordinates that have a common set of frequencies (or common support), provides robust estimation of the sampling interval. Fourier descriptors are then estimated by a least-squares fit. We have shown that the variances of the estimates meet the corresponding Cramér-Rao lower bounds at SNRs above 20 dB. We also demonstrate applications of the proposed FRI-FD method to reliably reconstruct the shape contours on some real images.

6. REFERENCES

[1] S. Belongie, J. Malik, and J. Puzicha, "Shape matching and object recognition using shape contexts," Tech. Rep., Department of Computer Science and Engineering, California University, San Diego, 2002.

[2] R. L. Cosgriff, "Identification of shape," Tech. Rep., Ohio State Univ. Res. Foundation, Columbus, Rep. 820-11, ASTIA AD 254 792, 1960.

[3] C. T. Zahn and R. Z. Roskies, "Fourier descriptors for plane closed curves," *IEEE Trans. Comput.*, vol. 100, no. 3, pp. 269–281, 1972.

[4] E. Persoon and K. Fu, "Shape discrimination using Fourier descriptors," *IEEE Trans. Syst., Man, Cybern.*, vol. 7, no. 3, pp. 170–179, 1977.

[5] E. Persoon and K. Fu, "Shape discrimination using Fourier descriptors," *IEEE Trans. Pattern Anal. Mach. Intell.*, vol. 8, no. 3, pp. 388–397, 1986.

[6] L. J. Latecki, R. Lakamper, and T. Eckhardt, "Shape descriptors for non-rigid shapes with a single closed contour," in *Proc. IEEE Int. Conf. Comput. Vis. Pattern Recognit.*, 2000, pp. 424–429.

[7] P. E. Lestrel, *Fourier Descriptors and Their Applications in Biology.* Cambridge University Press, 2008.

[8] V. F. Leavers, *Shape Detection in Computer Vision Using the Hough Transform.* New York: Springer-Verlag, 1992.

[9] J. Cheng, W. Huang, S. Cao, R. Yang, W. Yang, Z. Yun, Z. Wang, and Q. Feng, "Enhanced performance of brain tumor classification via tumor region augmentation and partition," *PLoS One*, vol. 10, no. 10, 2015.

[10] J. Cheng, W. Yang, M. Huang, W. Huang, J. Jiang, Y. Zhou, R. Yang, J. Zhao, Y. Feng, Q. Feng, et al., "Retrieval of brain tumors by adaptive spatial pooling and Fisher vector representation," *PLoS One*, vol. 11, no. 6, 2016.

[11] I. Giotis, N. Molders, S. Land, M. Biehl, M. F. Jonkman, and N. Petkov, "MED-NODE: A computer-assisted melanoma diagnosis system using non-dermoscopic images," *Expert Systems with Applications*, vol. 42, no. 19, pp. 6578–6585, 2015.

[12] M. Vetterli, P. Marziliano, and T. Blu, "Sampling signals with finite rate of innovation," *IEEE Trans. Signal Process.*, vol. 50, no. 6, pp. 1417–1428, Jun. 2002.

[13] S. Mulleti and C. S. Seelamantula, "Ellipse fitting using the finite rate of innovation sampling principle," *IEEE Trans. Image Process.*, vol. 25, no. 3, pp. 1451–1464, 2016.

[14] P. Stoica and R. L. Moses, *Introduction to Spectral Analysis.* Upper Saddle River, NJ: Prentice Hall, 1997.

[15] G. R. deProny, "Essai experimental et analytique: Sur les lois de la dilatabilité de fluides élastiques et sur celles de la force expansive de la vapeur de l'eau et de la vapeur de l'alcool, à différentes températures," *J. de l'Ecole Polytechnique*, vol. 1, no. 2, pp. 24–76, 1795.

[16] H. Pan, T. Blu, and P. L. Dragotti, "Sampling curves with finite rate of innovation," *IEEE Trans. Signal Process.*, vol. 62, no. 2, pp. 458–471, 2014.

[17] G. Ongie and M. Jacob, "Super-resolution MRI using finite rate of innovation curves," in *Proc. IEEE Int. Symp. Biomed. Imag. (ISBI)*, 2015, pp. 1248–1251.

[18] G. Ongie and M. Jacob, "Off-the-grid recovery of piecewise constant images from few Fourier samples," *SIAM J. Imaging Sci.*, vol. 9, no. 3, pp. 1004–1041, 2016.

[19] G. Ongie and M. Jacob, "A fast algorithm for convolutional structured low-rank matrix recovery," *IEEE Trans. Comput. Imag.*, vol. 3, no. 4, pp. 535–550, 2017.

[20] R. Tur, Y. C. Eldar, and Z. Friedman, "Innovation rate sampling of pulse streams with application to ultrasound imaging," *IEEE Trans. Signal Process.*, vol. 59, no. 4, pp. 1827–1842, Apr. 2011.

[21] C. S. Seelamantula and S. Mulleti, "Super-resolution reconstruction in frequency-domain optical-coherence tomography using the finite-rate-of-innovation principle," *IEEE Trans. Signal Process.*, vol. 62, no. 19, pp. 5020–5029, Oct. 2014.

[22] O. Bar-Ilan and Y. C. Eldar, "Sub-Nyquist radar via Doppler focusing," *IEEE Trans. Signal Process.*, vol. 62, no. 7, pp. 1796–1811, Apr. 2014.

[23] S. Rudresh and C. S. Seelamantula, "Finite-rate-of-innovation-sampling-based super-resolution radar imaging," *IEEE Trans. Signal Process.*, vol. 65, no. 19, pp. 5021–5033, 2017.

[24] Y. Barbotin, A. Hormati, S. Rangan, and M. Vetterli, "Estimation of sparse MIMO channels with common support," *IEEE Trans. Commun.*, vol. 60, no. 12, pp. 3705–3716, Dec. 2012.

[25] C. C. Lin and R. Chellappa, "Classification of partial 2-D shapes using Fourier descriptors," *IEEE Trans. Pattern Anal. Mach. Intell.*, vol. 9, no. 5, pp. 686–690, 1987.

[26] J. Canny, "A computational approach to edge detection," *IEEE Trans. Pattern Anal. Mach. Intell.*, vol. 8, no. 6, pp. 679–698, 1986.